ChemPubSoc Europe

DOI: 10.1002/open.201402112

Open Access ChemistryOPEN Communications

Ferric Phosphate Hydroxide Microstructures Affect Their Magnetic Properties

Junhong Zhao,[a] Youjuan Zhang,[a] Zhen Run,[a] Pengwei Li,[a] Qifei Guo,[a] and Huan Pang*[a, b]

Uniformly sized and shape-controlled nanoparticles are important due to their applications in catalysis, electrochemistry, ion exchange, molecular adsorption, and electronics. Several ferric phosphate hydroxide ($Fe_4(OH)_3(PO_4)_3$) microstructures were successfully prepared under hydrothermal conditions. Using controlled variations in the reaction conditions, such as reaction time, temperature, and amount of hexadecyltrimethylammonium bromide (CTAB), the crystals can be grown as almost perfect hyperbranched microcrystals at 180 °C (without CTAB) or relatively monodisperse particles at 220 °C (with CTAB). The large hyperbranched structure of $Fe_4(OH)_3(PO_4)_3$ with a size of ~19 μm forms with the "fractal growth rule" and shows many branches. More importantly, the magnetic properties of these materials are directly correlated to their size and micro/nanostructure morphology. Interestingly, the blocking temperature (T_B) shows a dependence on size and shape, and a smaller size resulted in a lower T_B. These crystals are good examples that prove that physical and chemical properties of nano/microstructured materials are related to their structures, and the precise control of the morphology of such functional materials could allow for the control of their performance.

A considerable amount of research has recently focused on the synthesis of uniformly sized and shape-controlled nanoparticles due to their potential applications in catalysis, electrochemistry, ion exchange, molecular adsorption, and electronics. Such nanoparticles are especially important for their magnetic properties, which are very sensitive to shape variation because of the dominant role of anisotropy in magnetism.[1] This prompts scientists to continuously develop new physical and chemical preparation methods for such materials. Different methods have already been developed to produce nanomaterials; among them, solution-based methods have been recognized as effective ways in designing the morphology and properties of nanomaterials.

The hyperbranched structure commonly has a wide range of size scales across examples in nature. Hyperbranched crystals, such as well-defined α-ferric oxide dendritic fractals and lead(II) sulfide three-dimensional dendritic nanostructures have already been obtained.[2–3] However, Xie et al.[4] reported that low crystal symmetry (monoclinic) is uncommon in nature. Thus it is a challenge for material scientists to find simple and reliable methods for the controlled synthesis of hierarchically hyperbranched architectures of low-crystal-symmetry materials that have designed chemical components and expected functionalities.

As some of the most promising iron-based materials, ferric phosphate hydroxide and ferric phosphate have recently attracted increased interest for their use in catalysts, wastewater purification systems, ferroelectrics, and lithium batteries.[4–10] Literature shows several iron phosphate phases exist due to complex formation reactions in the iron(III) ion–phosphate ion system.[11] Different synthetic routes to ferric phosphate hydroxide or ferric phosphate have been reported;[4,12–16] however, the fabrication of ferric phosphate hydroxide or ferric phosphate nano/micromaterials with controlled morphology is still a challenge.

Herein, we have successfully synthesized several hyperbranched ferric phosphate hydroxide ($Fe_4(OH)_3(PO_4)_3$) microstructures under hydrothermal conditions. More importantly, by controlling the reaction conditions, the microcrystals can be grown into relatively monodisperse or almost perfect hyperbranched $Fe_4(OH)_3(PO_4)_3$ microcrystals. Their magnetic properties are directly correlated with their sizes and micro/nanostructures. It is interesting that the blocking temperature (T_B) depends on size and shape, e.g. smaller size resulted in a lower T_B value.

Table 1 and the Supporting Information show detailed experimental parameters and the corresponding sample names. We obtained five samples by changing the reaction time, tem-

Table 1. Experimental parameters for the five samples.

Sample	Chemical agents				Hydrothermal conditions	
	$Fe(NO_3)_3{\cdot}9H_2O$ [g]	$Na_3PO_4{\cdot}12H_2O$ [g]	CTAB [g]	H_2O [mL]	Temp [°C]	Time [h]
N1	0.202	0.19	0	20	180	16
N2	0.202	0.19	0	20	180	24
N3	0.202	0.19	0	20	220	16
N4	0.202	0.19	0.5	20	220	16
N5	0.202	0.19	0.5	20	220	24

[a] *Dr. J. Zhao, Y. Zhang, Z. Run, P. Li, Q. Guo, Prof. H. Pang*
College of Chemistry and Chemical Engineering, Anyang Normal University
Anyang, Henan, 455002 (P. R. China)
E-mail: huanpangchem@hotmail.com
Homepage: http://huanpangchem.wix.com/advanced-material

[b] *Prof. H. Pang*
State Key Laboratory of Coordination Chemistry, Nanjing University
Nanjing, Jiangsu, 210093 (P. R. China)

Supporting information for this article is available on the WWW under http://dx.doi.org/10.1002/open.201402112.

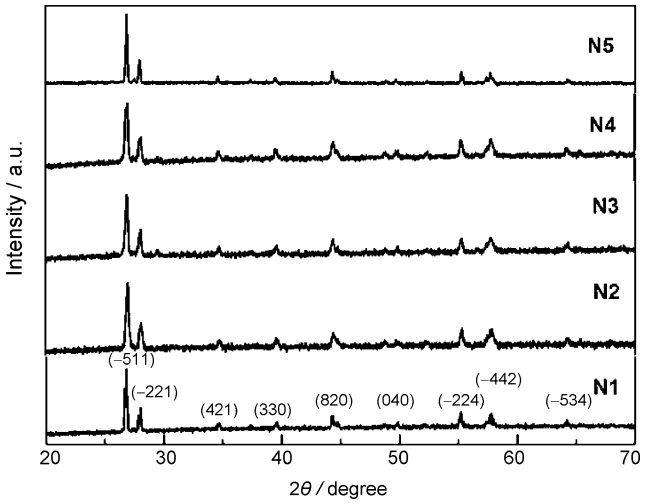

Figure 1. XRD patterns of as-prepared $Fe_4(OH)_3(PO_4)_3$ samples **N1**–**N5**.

perature, or amount of hexadecyltrimethylammonium bromide (CTAB). Figure 1 shows X-ray diffraction (XRD) patterns of as-prepared samples **N1**–**N5**. All peaks of the pattern are confirmed to be in agreement with $Fe_4(OH)_3(PO_4)_3$ (Joint Committee on Powder Diffraction Standards (JCPDS) No. 81-1346, Monoclinic, Cell: $a=19.58$, $b=7.388$, $c=7.451$), which is the same as the report of Xie et. al.[4] No peaks of other phosphites or phosphates were detected from these patterns. The peaks are strong and narrow, which indicate the good crystallinity of the as-prepared samples. The addition of the CTAB does not affect the crystallinity of the obtained sample. However, CTAB may be absorbed on different crystal facets which results in the different morphologies obtained.

Figures 2 a, b display typical scanning electron microscopy (SEM) images of the product **N1** prepared with $Fe(NO_3)_3{\cdot}9H_2O$ (0.202 g) and $Na_3PO_4{\cdot}12H_2O$ (0.19 g) in H_2O (20 mL) at 180 °C for 16 h. From these images, it could easily be seen that the product is composed of hexa-cone hyperbranched structures with a size of ~8–9 μm. The high magnification image of **N1** clearly shows that the hexa-cone hyperbranched microcrystal is perfect with a smooth surface and six branches. Further reactions with prolonged time and increased temperature were then done. Figures 2 c, d show SEM images of the product **N2** prepared with $Fe(NO_3)_3{\cdot}9H_2O$ (0.202 g) and $Na_3PO_4{\cdot}12H_2O$ (0.19 g) in H_2O (20 mL) at 180 °C for 24 h, which is the same as earlier conditions except for a prolonged reaction time of 24 h. **N2** is also composed of hexa-cone hyperbranched structures with a size of ~17 μm, but single branches are slimmer. More importantly, the surfaces are uneven and rough, which is probably due to the prolonged reaction time and growth of crystals. Figures 2 e, f show SEM images of the product **N3** prepared under the same conditions as for **N1** but with an increased temperature of 220 °C. **N3** was found to have a larger hyperbranched structure with a size of ~19 μm formed with the "fractal growth rule". There are many branches, and each branch is composed of a great number of naturally symmetrical nanocrystals in as seen in Figure 2 f.

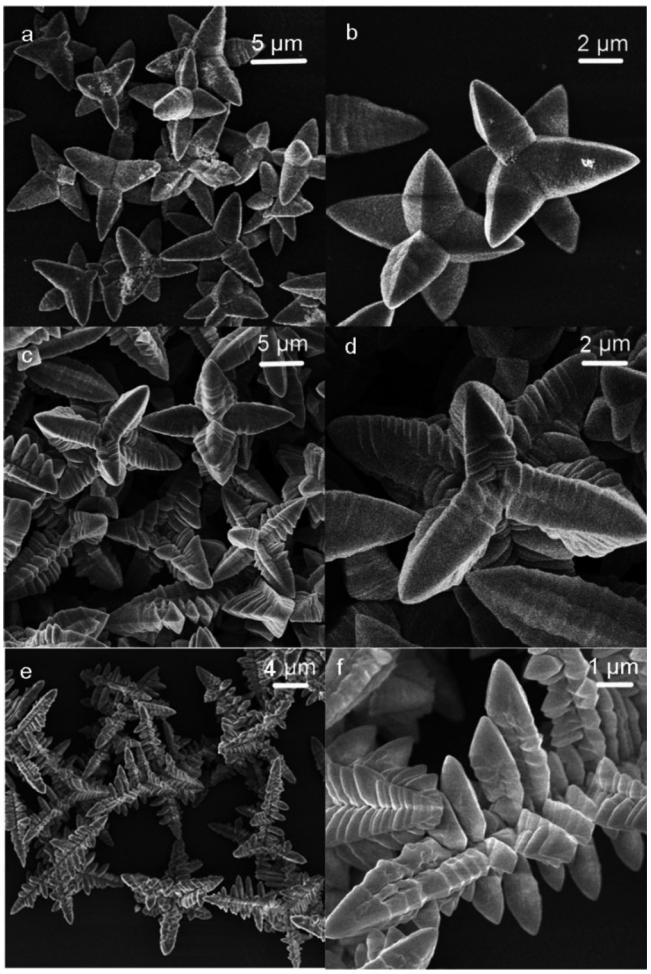

Figure 2. SEM images of as-prepared $Fe_4(OH)_3(PO_4)_3$ samples. a,b) **N1**, c,d) **N2**, and e,f) **N3**.

Figures 3 a, b show SEM images of the product **N4** prepared under the same conditions as **N3** (shown in Figures 2 e, f) except for the addition of CTAB (0.50 g) into the reaction. The morphology of as-prepared sample **N4** changed into a corner-truncated octahedron with a size of ~6.5 μm. From this, it is obvious that the CTAB affects the growth of the product.[4] Using the reaction conditions for **N4** but increasing the reaction time to 24 h, we get as-prepared sample **N5**, with a microstructure reminiscent of a three-dimensional Christian Latin cross, which has a short horizontal axis and slightly longer vertical axis, but with the ends blunted. The CTAB is also important to form the Christian-cross morphology. The transformation from the corner-truncated octahedron to the Christian-cross morphology strongly depends on the competition between the etching and capping of surface of crystals by CTAB. The long reaction time makes CTAB etch and cap the corner-truncated octahedron to a large extent.[4] The etching tends to decompose the particles, whereas the adsorbed CTAB molecules stabilize the particle surface and prevent that specific crystal facet from being etched. Once a pit has formed on the surface, further corrosion would occur inside the pit preferentially. As etching continues, the concentration of phosphate

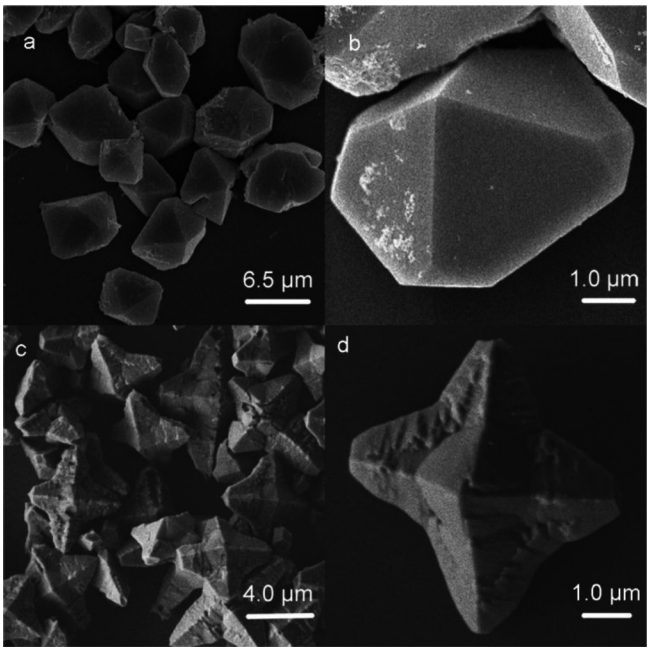

Figure 3. SEM images of as-prepared $Fe_4(OH)_3(PO_4)_3$ samples. a,b) **N4** and c,d) **N5**.

ions sufficiently decreases. In other words, the concentration of protons decreases and thus leads to the weakening of etching. As the etching and capping proceeds, the Christian-cross morphology forms. We propose three possible reactions under these hydrothermal conditions:

$$H_2O + PO_4^{3-} \rightleftharpoons HPO_4^{2-} + OH^- \quad (1)$$

$$4\,Fe^{3+} + 3\,PO_4^{3-} + 3\,OH^- \rightleftharpoons Fe_4(OH)_3(PO_4)_3 \quad (2)$$

$$Fe_4(OH)_3(PO_4)_3 + 5\,PO_4^{3-} \rightleftharpoons 4[Fe(PO_4)_2]^{3-} + 3\,OH^- \quad (3)$$

The magnetic properties of micro/nanomaterials are directly dependent on the size and shape of the particles. Understanding the correlation between micro/nanostructure and magnetic property is important for fundamental research, but also for the development of potential applications in electronic and information technologies. The size and shape-dependent magnetic properties of the five $Fe_4(OH)_3(PO_4)_3$ microcrystals (**N1**–**N5**) were studied using a superconducting quantum interference device (SQUID). Zero-field-cooled–field-cooled (ZFC–FC) temperature scanning at 500 Oe is shown in Figure 4 and Figure S1 in the Supporting Information. The five $Fe_4(OH)_3(PO_4)_3$ samples have ferrimagnetic behavior at low temperatures as shown in Figure 4. ZFC measurement was carried out, cooling from 300 to 1.8 K without any external magnetic field. Then a magnetic field of 500 Oe was applied, and the magnetization of the sample was measured following the rise in the temperature. When the temperature approaches a specific point, the magnetization reaches a maximum and then starts to decrease. The specific temperature point at which the thermal activation overcomes all the energy barriers is known as the blocking temperature (T_B). Moreover, in the FC measurement,

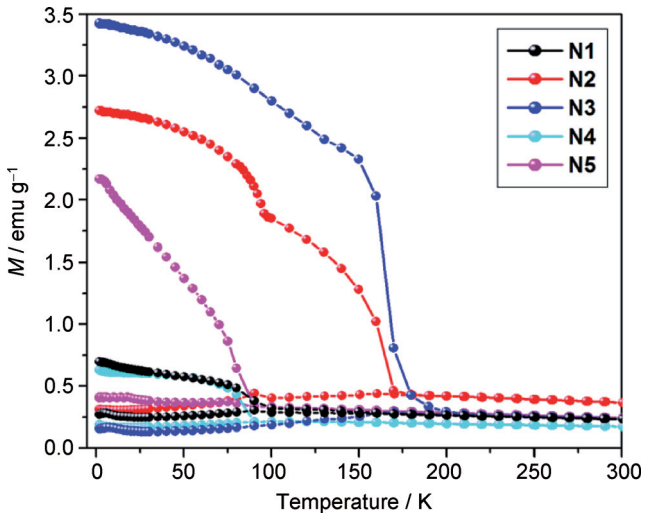

Figure 4. The sum of zero-field-cooled–field-cooled (ZFC–FC) temperature scan at 500 Oe for **N1**–**N5**.

the sample was initially cooled to 1.8 K under an applied magnetic field of 500 Oe. The subsequent magnetization measurement was recorded from 1.8 to 300 K with the magnetic field kept at 500 Oe (Figure 4). The T_B of as-prepared $Fe_4(OH)_3(PO_4)_3$ microcrystals is shown in Table 2. The biggest crystal, **N3,** has

Table 2. Magnetic data obtained from Figures 4 and 5.

Sample	T_B[a] [K]	M_{max}[b] [emu g^{-1}]	M_r[c] [emu g^{-1}]	H_c[d] [Oe]
N1	89.9	10.30	0.53	1038.00
N2	98.9	18.40	1.80	1183.00
N3	170.3	31.20	3.90	6460.00
N4	76.9	3.70	0.43	874.00
N5	75.5	10.30	0.51	909.00

[a] T_B: blocking temperature; [b] M_{max}: maximum magnetization; [c] M_r: saturation magnetization; [d] H_c: coercivity.

the highest T_B (170.3 K) among the five, while the smallest crystal, **N5,** has the lowest one (75.5 K). It is interesting that the T_B shows size and shape dependence, and that a smaller size results in a lower T_B value. A similar behavior has been documented for other types of nanoparticles, for example, nickel and terbium.[17–19]

Although the hysteresis loop was obtained at 1.8 K in a magnetic field of up to ±60 kOe (Figure 5 and Figure S2 in the Supporting Information), the saturation magnetization (M_s) of as-prepared hyperbranched $Fe_4(OH)_3(PO_4)_3$ was not reached. The maximum magnetization (M_{max}) of as-prepared hyperbranched $Fe_4(OH)_3(PO_4)_3$ is also shown in Table 2. **N3** has the largest value (31.2 emu g^{-1}), while **N4** has the smallest (3.70 emu g^{-1}). Furthermore, a remanence ratio (M_r/M_{max}) of 12.50% for **N3** was estimated in Table 2. The coercivity (H_c) for hyperbranched $Fe_4(OH)_3(PO_4)_3$ is also affected by its size and shape, and **N3** also shows the largest H_c at 6460 Oe which is eight times that of the smallest, **N4**.

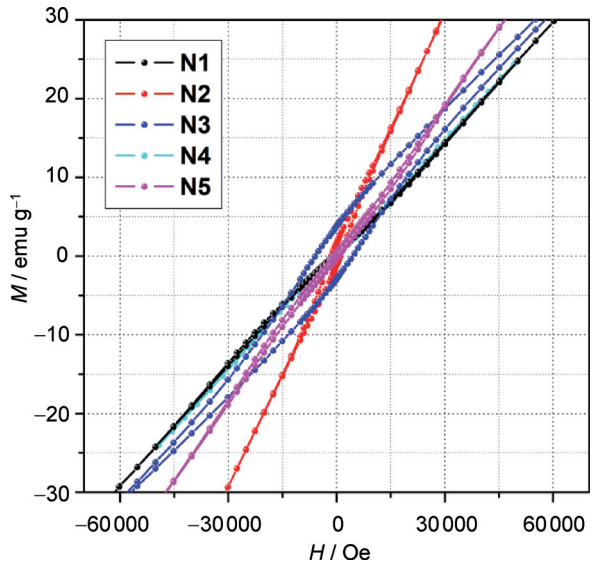

Figure 5. The magnetic hysteresis loop at 1.8 K of as-prepared samples **N1**–**N5** from −60000 Oe to 60000 Oe.

As expected, the magnetic behavior is influenced by the hyperbranched structure and size. A principal effect of specific micro/nanostructure and size is the breaking of a large number of bonds on the surface cations, producing a core of aligned spins surrounded by a disordered shell. This can result in a disordered spin configuration near the surface and a reduced average net moment compared to bulk materials. In addition, the surface spin states can result in high-field hysteresis and relaxation of the magnetization,[20] as has been observed for these micro/nanostructures.

In summary, several hyperbranched $Fe_4(OH)_3(PO_4)_3$ samples have been successfully prepared under hydrothermal conditions. Varying growth parameters, such as reaction time, temperature and CTAB content significantly influences the shape and size of as-prepared $Fe_4(OH)_3(PO_4)_3$ microcrystals. More importantly, the magnetic properties of these nanocrystals are very sensitive to their size and shape. These T_B phenomena are expected to result from the effects of the finite size and the volume of particles. These crystals are good examples that prove that physical and chemical properties of nano/microstructured materials are related to their structures, and the precise control of the morphology of such functional materials could allow for the control of their performance.

Acknowledgements

This work is supported by the Program for New Century Excellent Talents (NCET-13-0645) the National Natural Science Foundation of China (NSFC-21201010, U1304504), the Science & Technology Foundation of Henan Province (122102210253, 13A150019, 14A430038), and the China Postdoctoral Science Foundation (2012M521115).

Keywords: blocking temperature · ferric phosphate hydroxide · hydrothermal condition · magnetic properties · microstructures

[1] H. Pang, Y. Y. Liu, Y. H. Ma, G. C. Li, Y. N. Ai, J. Chen, J. S. Zhang, H. H. Zheng, *Nanoscale* **2013**, *5*, 503–507.
[2] M. H. Cao, T. F. Liu, S. Gao, G. B. Sun, X. L. Wu, C. W. Hu, Z. L. Wang, *Angew. Chem. Int. Ed.* **2005**, *44*, 4197–4201; *Angew. Chem.* **2005**, *117*, 4269–4273.
[3] D. Kuang, A. Xu, Y. Fang, H. Liu, C. Frommen, D. Fenske, *Adv. Mater.* **2003**, *15*, 1747–1750.
[4] Y. Zhao, Y. Xie, X. Zhu, S. Yan, S. X. Wang, *Chem. Eur. J.* **2008**, *14*, 1601–1606.
[5] Y. Zhao, Y. Xie, S. Yan, X. Zhu, *Chem. Mater.* **2008**, *20*, 3959–3964.
[6] D. Li, C. S. Pan, R. Shi, Y. F. Zhu, *CrystEngComm* **2011**, *13*, 6688–6693.
[7] S. Scaccia, M. Carewska, P. P. Prosini, *Thermochim. Acta* **2004**, *413*, 81–86.
[8] X. L. Li, W. J. Wei, S. Z. Wang, L. Kuai, B. Y. Geng, *Nanoscale* **2011**, *3*, 718–724.
[9] K. X. Wang, J. H. Yu, Y. Song, R. R. Xu, *Dalton Trans.* **2003**, 99–103.
[10] Y. H. Ni, K. M. Liao, J. M. Hong, X. W. Wei, *CrystEngComm* **2009**, *11*, 570–575.
[11] C. Masquelier, A. K. Padhi, K. S. Nanjundaswamy, J. B. Goodenough, *J. Solid State Chem.* **1998**, *135*, 228–234.
[12] G. Lente, M. Elizabeth, A. Magalhaes, I. Fabian, *Inorg. Chem.* **2000**, *39*, 1950–1954.
[13] S. Z. Wang, Q. Wang, J. Liu, Z. G. Cheng, D. J. Si, B. Y. Geng, *CrystEngComm* **2009**, *11*, 2510–2515.
[14] S. Scaccia, M. Carewska, A. D. Bartolomeo, P. P. Prosini, *Thermochim. Acta* **2003**, *397*, 135–141.
[15] C. Delacourt, C. Wurm, P. Reale, M. Morcrette, C. Masquelier, *Solid State Ionics* **2004**, *173*, 113–118.
[16] T. B. Zhang, Y. C. Lu, G. S. Luo, *CrystEngComm* **2013**, *15*, 9104–9111.
[17] S. M. Zhang, J. X. Zhang, S. J. Xu, X. J. Yuan, T. Tan, *J. Power Sources* **2013**, *243*, 274–279.
[18] D. Johnson, R. Perera, M. J. Oshea, *J. Appl. Phys.* **1996**, *79*, 5299–5301.
[19] K. Y. Mulyukov, R. Z. Valiev, G. F. Korznikova, V. V. Stolyarov, *Phys. Status Solidi* **1989**, *112*, 137–143.
[20] N. N. Zhao, W. Nie, X. B. Liu, S. Z. Tian, Y. Zhang, X. L. Ji, *Small* **2008**, *4*, 77–81.
[21] R. H. Kodama, *J. Magn. Magn. Mater.* **1999**, *200*, 359–372.

Received: November 15, 2014
Published online on January 12, 2015

